Earth Science Informatics (2021) 14:1111–1120
https://doi.org/10.1007/s12145-021-00619-0

REVIEW ARTICLE

Impact of elevation mask on multi-GNSS precise point positioning performance

Yi bin Wu[1] · Yanyan Liu[1,2] · Wenting Yi[2] · Hong bin Ge[3]

Received: 23 March 2020 / Accepted: 12 April 2021 / Published online: 12 May 2021
© The Author(s), under exclusive licence to Springer-Verlag GmbH Germany, part of Springer Nature 2021

Abstract

Precise point positioning (PPP) is famous for its capability of high-precision positioning and its wide application in many fields. With the rapid development of BDS and Galileo, the number of GNSS satellites used for positioning has now exceeded 110. It brings both opportunities and challenges to PPP. Based on the data of 90 tracking stations of MGEX, this paper analyzed the impact of elevation masks on the performance of multi-GNSS kinematic PPP. The results show that the PODP increases as the elevation mask increases. In general, it will reduce the positioning accuracy and the convergence speed with the increasing of the elevation mask for the PPP float solution. Furthermore, when the elevation mask is below 25°, increasing the elevation mask has little effect on the position accuracy of the horizontal and vertical components in the first 10 min. But after 15 min, the effect on the vertical component became apparently. And after convergence, the RMS of multi-GNSS PPP float solution can reach 5 cm and 10 cm for the horizontal and vertical components when the elevation mask is below 25°. When the elevation mask is 30°, the RMS is still less than 6 cm for the horizontal component, while about 99% of the RMS is less than 11.5 cm for the vertical component. Thirdly, for multi-GNSS PPP AR, it can improve the TTFF and the fixing percentage by fixing the ambiguity subnet with higher elevation mask firstly. Moreover, when the elevation mask is below to 20°, the improvement is more obvious and when the elevation mask is larger than 25°, the TTFF may become longer in some cases.

Keywords Multi-GNSS · PPP · Elevation mask · Convergence · Positioning accuracy · PDOP · TTFF · Fixing percentage

Introduction

Precise Point Positioning (PPP) can achieve positioning accuracy for static and mobile receivers at the millimeter to decimeter levels in the whole world without the need for a nearby reference station and has been widely applied in geodesy, precise navigation and location based service, precise timing, precise agriculture and aerial photogrammetry (Zumberge et al. 1997; Kouba 2003; Bisnath and Gao 2008;Guo et al. 2018). However, PPP has long time been based on GPS-only PPP with float ambiguity solution and it needs an initialization time of more than 30 min to achieve centimeter-level positioning accuracy. In order to improve the positioning accuracy and shorten the initialization time, PPP ambiguity resolution (AR) technique has been developed in recent years (Ge et al. 2008; Collins et al. 2008; Laurichesse et al. 2009). The results show that compared with float solution, the dual-frequency GPS PPP AR solution can improve the 3D positioning accuracy by 54% from 4.8 to 2.2 cm, and shorten the convergence time by 32% from 31.6 to 21.4 min (Li et al. 2013).

✉ Yanyan Liu
whdxlyy@qq.com

Yi bin Wu
53686090@qq.com

Wenting Yi
ywtsky1985@163.com

Hong bin Ge
360396054@qq.com

[1] Department of Civil Engineering and Architecture, Xiamen University of Technology, Xiamen 36102, China

[2] Shenzhen Key Laboratory of Spatial Smart Sensing and Services, College of Civil Engineering, Shenzhen University, 3688 nanhai road, Shenzhen 518060, Guangdong, China

[3] Xiamen Xiang'an airport investment and Construction Co., Ltd, Xiamen 36102, China

With the rapid development of GLONASS, BDS and Galileo, the International GNSS Service (IGS) has established the multi-GNSS experiment (MGEX) since 2012, which aims to provide multi-GNSS data service of observations, precise orbit and precise clock offset products (Montenbruck et al. 2017). Based on the data products, the performance of multi-GNSS PPP with dual/trip/quad-constellation satellites was studied. It is proved that multi-GNSS PPP is superior to GPS-only PPP both in the positioning accuracy and convergence time (Li and Zhang 2014; Li et al. 2015; Cai et al. 2015; Lou et al. 2016; Rabbou and Elrabbany 2017; An et al. 2020). Similarly, multi-GNSS PPP ambiguity resolution (PPP AR) can also be improved. Liu et al. (2017) experimented on a regional network and reported that 90% of GPS/GLONASS/BDS PPP ambiguities could be fixed within 10 min, whereas only 16% for GPS-only ambiguities; Nadarajah et al. (2018) showed that the convergence time in case of Australia-wide GPS/BDS/Galileo PPP AR was reduced from 66 to 15 min. Li et al. (2018) proved that PPP AR with quad-constellation satellite enables the fastest time to first fix (TTFF) solutions and the highest accuracy for all three coordinate components compared to the single and dual system. When the elevation mask is increased to 30°, the GPS-only PPP AR results are very unreliable, while 13.44 min of TTFF is still achievable for quad-constellation solutions.

However, for the multi-GNSS PPP AR with quad-constellation satellites, due to the increasing of ambiguity parameters, it will increases the computational burden and reduces the ambiguity fixing rate significantly to fix all the ambiguities. Therefore, the partial ambiguity fixing methods are proposed (Teunissen et al. 1999; Parkins 2011; Henkel and Günther 2012; Wang and Feng 2013; Brack and Günther 2014). How to choose the best ambiguity subnet is important for partial ambiguity fixing and the simplest way is to choose the ambiguity subset according to the elevation mask. But how to choose the best elevation mask is still need to be investigated. Therefore, this paper evaluated the impact of the elevation mask on the performance of GPS/GLONASS/Galileo/BDS multi-GNSS kinematic PPP. In this paper, we used both BDS-2 and BDS-3 data. The rest of this paper is organized as follows. Section 2 gives the multi-GNSS PPP model and data process strategy. Section 3 analyzes the PDOP of multi-GNSS PPP at different elevation masks. Section 4 analyzes the performance of multi-GNSS PPP at different elevation masks based on the data of 90 individual MGEX stations. Section 5 presents some preliminary results and discusses.

Multi-GNSS PPP mathematical model and the data process strategy

In double frequency GNSS data processing, the ionosphere-free combination is usually used to eliminate the first order of the ionospheric delay. The pseudorange and carrier phase ionosphere-free combination observation can be expressed as:

$$\begin{cases} P_{if}^{S,i} = \rho + c\Delta t^{i} - c\Delta t_{r,S} + \delta_{Trop} + \varepsilon\left(P_{if}^{S,i}\right) \\ \Phi_{if}^{S} = \rho + c\Delta t^{i} - c\Delta t_{r,S} + \delta_{Trop} + \lambda_i N^{i} + \varepsilon\left(\Phi_{if}^{S,i}\right) \end{cases} \tag{1}$$

Where S refers GNSS system, i is the satellite PRN, $P_{if}^{S,i}$, $\Phi_{if}^{S,i}$ are the ionosphere-free pseudorange and carrier phase observation in meters; $\rho$is the range from satellite to receiver including systematic errors such as solid earth tides, Sagnac delay, windup and so on; c is the speed of light in vacuum; Δt^{i} is the satellite clock bias; $\Delta t_{r,S}$ is the receiver clock bias; δ_{Trop} is the zenith troposphere delay; λ_i is the signal wavelength, N is the integer carrier phase ambiguity; $\varepsilon\left(P_{if}^{S,i}\right)$, $\varepsilon\left(\Phi_{if}^{S,i}\right)$ refers to the uncorrected systematic and random pseudorange and carrier phase errors.

We used the WUM final orbit and clock products released by Wuhan university to eliminate the orbit and clock bias. The dry components of the troposphere, solid earth tides, Sagnac delay, etc. were corrected using high-precision models, whereas the wet components of the troposphere were estimated by the random walk method. Therefore, the observation equations for multi-GNSS double-frequency PPP can be written as follows:

$$\begin{cases} P_{if}^{G,i} = \rho - c\Delta_{r,G} + \delta_{Trop} + \varepsilon\left(P_{if}^{G,i}\right) \\ P_{if}^{R,j} = \rho - c\Delta_{r,R} + \delta_{Trop} + \varepsilon\left(P_{if}^{R,j}\right) \\ P_{if}^{E,l} = \rho - c\Delta_{r,E} + \delta_{Trop} + \varepsilon\left(P_{if}^{E,l}\right) \\ P_{if}^{C,m} = \rho - c\Delta_{r,C} + \delta_{Trop} + \varepsilon\left(P_{if}^{C,m}\right) \\ \Phi_{if}^{G} = \rho - c\Delta t_{r,G} + \delta_{Trop} + \lambda_i N^{i} + \varepsilon\left(\Phi_{if}^{G,i}\right) \\ \Phi_{if}^{R,j} = \rho - c\Delta t_{r,R} + \delta_{Trop} + \lambda_j N^{j} + \varepsilon\left(\Phi_{if}^{R,j}\right) \\ \Phi_{if}^{E,l} = \rho - c\Delta t_{r,E} + \delta_{Trop} + \lambda_l N^{l} + \varepsilon\left(\Phi_{if}^{E,l}\right) \\ \Phi_{if}^{C,m} = \rho - c\Delta t_{r,C} + \delta_{Trop} + \lambda_m N^{m} + \varepsilon\left(\Phi_{if}^{C,m}\right) \end{cases} \tag{2}$$

Where G, R, E, C refers GPS, GLONASS, Galileo and BDS, i, j, l, m is the satellite PRN, ρ is the range from satellite to receiver without systematic errors. To be consistency with orbit and clock products, in Eq. (2), the two frequencies selected to form the ionosphere-free combination are L1/L2 for GPS, G1/G2 for GLONASS, B1/B3 for BDS, and E1/E5a for Galileo.

The PPP float solution cannot make full use of the high-precision characteristics of carrier phase observations, which affects the positioning accuracy and initialization time of PPP (Ge et al. 2008;Geng et al. 2012). However, ambiguity integer characteristic can be recovered and the PPP AR can be obtained by using the un-calibration phase delay (UPD) (Ge et al. 2008). The PPP ambiguity is usually fixed by two-step, Wide-

Lane (WL) and Narrow-Lane (NL) ambiguity fixing (Ge et al. 2008). Firstly, the WL ambiguity is usually fixed by using Melbourne–Wübbena (MW) combined observations. Because the wavelength of MW combination observation is long, it is less affected by measurement noise and observation error. After several epochs of smoothing, the WL ambiguity can achieve higher accuracy, so the WL ambiguity can be fixed to the nearest integer directly (Ge et al. 2008). The NL float ambiguity can be obtained from ionosphere-free combination ambiguity and integer WL ambiguity according to Eq. (3):

$$N_{nl} = \frac{f_1 + f_2}{f_1} N - \frac{f_2}{f_1 - f_2} N_{wl} \tag{3}$$

Where f_1, f_2 refers the frequency of the L1 and L2 carrier phase observations. N_{nl}, N_{wl} refers he NL and WL ambiguity. Because the NL ambiguities obtained by PPP have strong correlation, NL ambiguity is fixed by least square ambiguity reduction correlation adjustment (LAMBDA) (Teunissen 1995). In this paper, the bootstrapping success rate (Teunissen 2007) and ratio test are used to check the ambiguity fixing and the bootstrapping success rate can be written as:

$$P = \prod_{i=1}^{n} \left(2\Phi \left(\frac{1}{2\sigma_{\widehat{N}_{i|I}}} \right) - 1 \right) \tag{4}$$

where $\Phi(x) = \frac{1}{\sqrt{2\pi}} \int_{-\infty}^{x} e^{-t^2/2} dt$, $\widehat{N}_{i|I}$ is short for $\widehat{N}_{i|i-1,\ldots,1}$, which is the conditional estimation of the i-th ambiguity with the condition that the previous (i-1) ambiguity is fixed to the integer value, $\sigma$is the standard deviation. If and only if the WL and NL ambiguities are fixed successfully, the ionosphere-free combination ambiguities with integer characteristics can be obtained can be obtained as:

$$N^{i,j} = \left(\frac{cf_2}{f_1^2 - f_2^2} N_{wl}^{i,j} + \frac{cf_2}{f_1^2 - f_2^2} \left(N_{nl}^{i,j} - upd_{nl}^{i,j} \right) \right) / \lambda \tag{5}$$

Where upd_{nl}refers NL UPD. By substituting Eq. (5) into Eq. (2) and eliminating the ambiguity parameter, the PPP ambiguity fixed solution can be obtained. The data process strategies are listed as follow (Table 1):

Analysis of multi-GNSS PPP PDOP

We used the multi-GNSS broadcast ephemeris, and compute the coordinates of each satellite every 2 h from DOY 349 to 355 in 2019. The Earth's surface is subdivided into a 1° × 1° grid with zero altitudes, and for the cell midpoints, we computed the elevations of the satellites. Then, for several

Table 1 The summary of the data processing strategies

A priori sigma of coordinates	A priori sigma of coordinates 100 m
A priori sigma of observations	1.0 m for pseudorange, 0.01 m for carrier phase
Frequencies	GPS, GLONASS: L1, L2; Galileo: E1, E5a; BDS: B1,B3
Observables weighting	Elevation (ε) dependent weighting:ε>=30,weight=1; 20<=ε<30, weight=sin(ε);10<=ε<20, weight=pow(sin(ε),2);
Receiver clock offset	estimated as white noise, a priori sigma=100 [m]
Troposphere delay modeling	A priori ZTD from UNB3 m model (Leandro et al. 2006); Global Mapping Function (Böhm et al. 2006); The residual is estimated as random walk.
Correction models	Phase wind-up (Wu et al. 1993), relativistic delays, solid earth tides, igs14_2072.atx,UPD(Hu et al. 2019)
Solution type	Coordinates estimated as white noise, with float ambiguities.

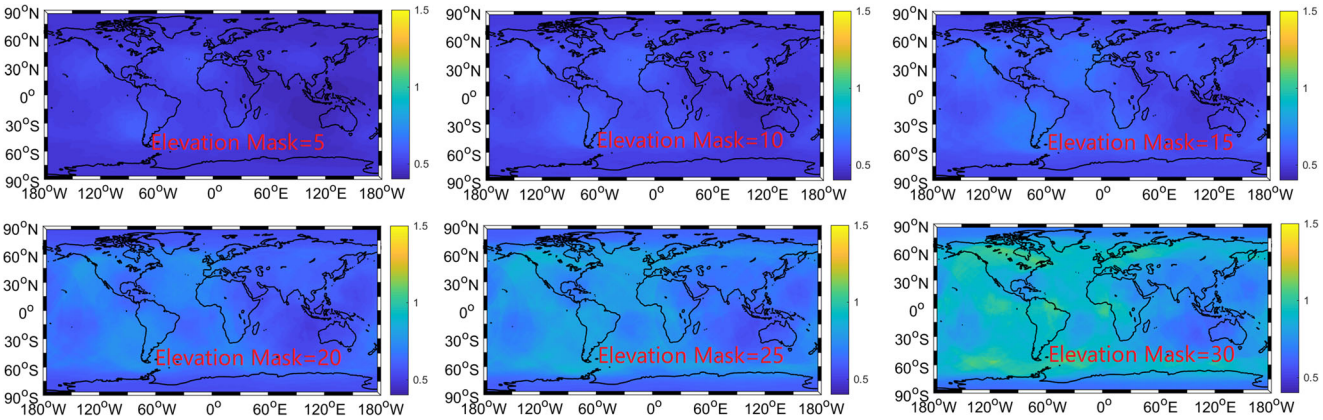

Fig. 1 The average PDOP with elevation masks of 5°, 10°, 15°, 20°, 25° and 30°

elevation masks and assuming no obstructions in view, we calculated the PDOP at each epoch. When fewer than four satellites were viewed, we skipped to calculate the PDOP.

We took the average of the PDOP over seven days. This allowed us to determine the average PDOP for each grid cell globally. Figure 1 shows the average PDOP with elevation masks of 5°, 10°, 15°, 20°, 25° and 30°. As shown in Fig.1, when the elevation mask is 5°, the average PDOP varies little in different regions. This means that the combined quad-constellation satellites can effectively make up for the deficiency of single constellation satellite in spatial dimension coverage. Therefore, the multi-GNSS PPP can obtain similar performance in different regions if there are no regional differences of the systemic errors, such as the ionospheric delay, orbit and clock offsets. As the elevation mask increases, the average PDOP increases and varies more and more obviously in different regions. The average PDOP is the best in the Asia-Pacific region because of BDS IGSO and GEO satellites. While several PDOP peak regions emerge firstly between about 20° ~ 50°north and between about 20° ~ 50°south. Then it exceeds to more and more regions with the elevation mask reach to 30°.

Figure 2 shows the PDOP probability distribution with elevation masks of 5°, 10°, 15°, 20°, 25° and 30°. As shown in Fig. 2, when elevation mask is below 15°, multi-GNSS PDOP is less than 1.0. When elevation mask is 20°, about

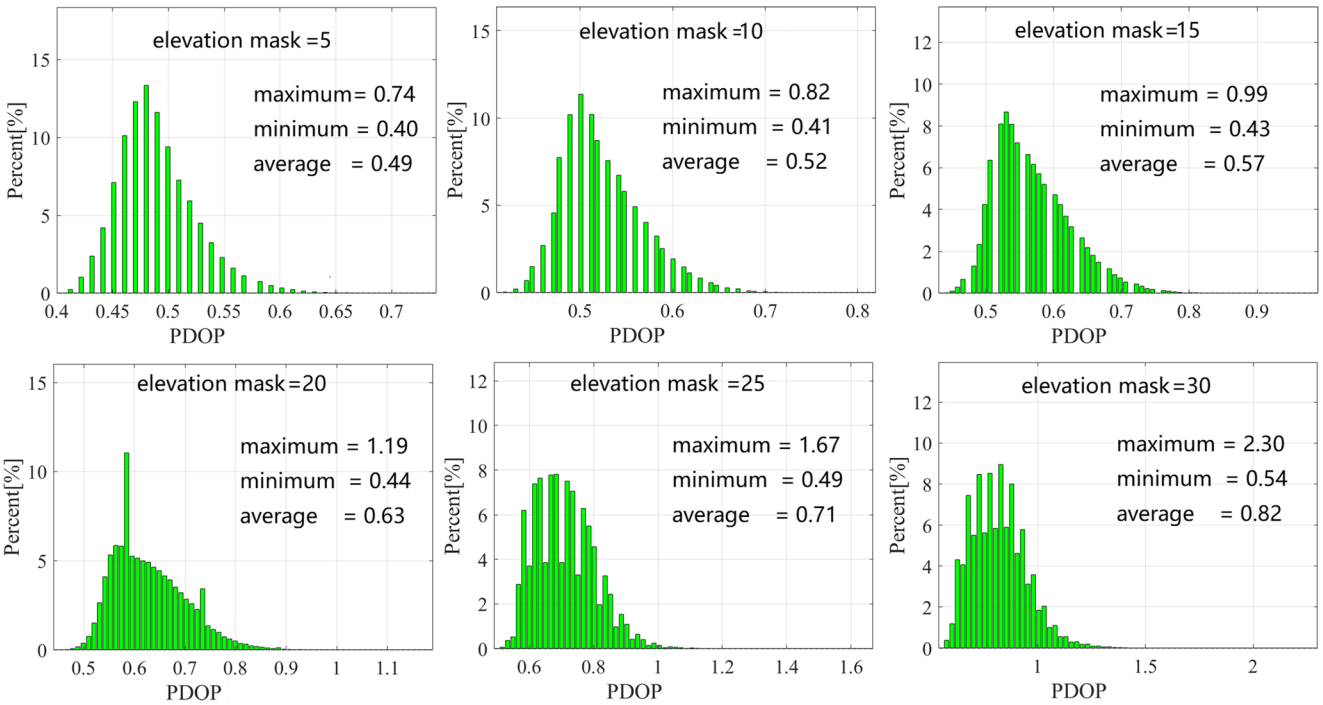

Fig. 2 The probability distribution of PDOP with elevation masks of 5°, 10°, 15°, 20°, 25° and 30°

98% PDOP is less than 1.0 and the maximum and average PDOP are 1.19 and 0.63. When the elevation mask is 30°, although the maximum PDOP can reach 2.3, there are still about 95% PDOP is less than 1.2 and the average PDOP is only 0.82.

The performance of the multi-GNSS kinematic PPP

To evaluate the impact of elevation masks on the performance of the multi-GNSS kinematic PPP, the data of 90 individual MGEX

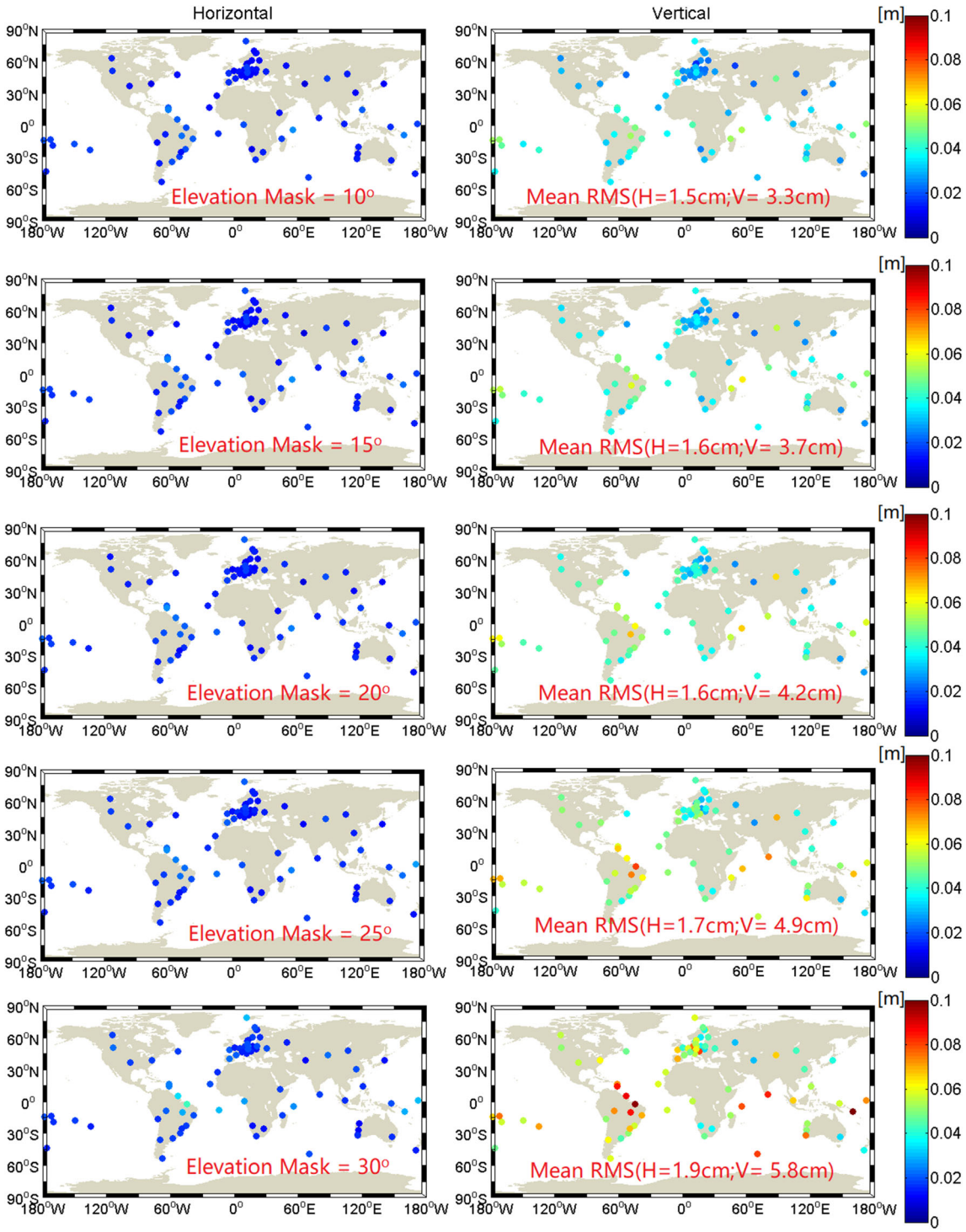

Fig. 3 the average RMS of multi-GNSS PPP with elevation masks of 10°, 15°, 20°, 25° and 30°

stations from 2019 DOY 349 to 355 were used for quad-constellation multi-GNSS PPP with elevation masks of 10°, 15°, 20°, 25° and 30°, respectively.

The performance of the multi-GNSS kinematic PPP float solution

Firstly, we analyzed the positioning accuracy and convergence time of the multi-GNSS kinematic PPP float solution and the real coordinate is provided by IGS weekly solutions. We took the average of the RMS for each station over a 7-day period. Fig. 3 shows the average RMS for the horizontal and vertical components with elevation masks of 10°, 15°, 20°, 25° and 30°. As shown in Fig. 3, the average RMS for the horizontal component varies little in different regions while for the vertical component, the average RMS of inland stations is smaller than that of stations near the sea. This is because the ocean tide model was not applied in this paper. In addition, with the increasing of the elevation mask, the positioning accuracy of the vertical component is significantly reduced, while hardly reduced of the horizontal component. When the elevation masks are set to 10°, 15°, 20°, 25° and 30°, the average RMS of the horizontal component reaches 1.5 cm, 1.6 cm, 1.6 cm, 1.7 cm and 1.9 cm, respectively, while the average RMS of the vertical component reaches 3.3 cm, 3.7 cm, 4.2 cm, 4.9 cm and 5.8 cm, respectively.

Furthermore, the RMS probability distribution with elevation masks of 10°, 15°, 20°, 25° and 30° were analyzed. The maximum RMS and the RMS in a confidence interval of 95% and 99% are listed in Table 2. When the elevation mask is below 25°, the multi-GNSS PPP positioning accuracy of the horizontal and vertical components is superior to 5 cm and 10 cm. When the elevation mask is 10°, for the horizontal component, the maximum RMS is 4.1 cm, and about 95% of the RMS is superior to 2.4 cm, while about 99% of the RMS is superior to 2.9 cm. For the vertical component, the maximum RMS is 8.3 cm, and about 95% of the RMS is superior to 5.6 cm, while about 99% of the RMS is superior to 6.6 cm. When the elevation mask reaches 30°, the positioning accuracy for the vertical component of some stations decreases, and the maximum RMS of the vertical component reaches 28.3 cm. Fortunately, there are still about 99% of RMS for the vertical component is superior to 11.5 cm and about 95% is superior to 9.2 cm. Moreover, the maximum RMS of the horizontal component is only 6 cm. and there is still about 95% of RMS of the horizontal component is superior to 3.1 cm and about 99% is superior to 5.3 cm.

To analyze the multi-GNSS PPP convergence time, the 24 h data were divided into 5, 8, 10, 15, 20, 30, 40 and 60 min to enlarge the data samples. Meanwhile, the positioning accuracy of multi-GNSS PPP, which in confidence intervals of 68.3% and 95%, and converge in 5, 8, 10, 15, 20, 30, 40 and 60 min, respectively, was used to evaluate the convergence time.

Figure 4 shows the positioning accuracy of multi-GNSS PPP with confidence intervals of 68.3% and 95% after 5, 8, 10, 15, 20, 30, 40 and 60 min convergence with elevation masks of 10°, 15°, 20°, 25° and 30°. As shown in Fig.6, as the elevation mask increase, it will affect the convergence time of multi-GNSS PPP. However, when the elevation mask is below 20°, the effect on the multi-GNSS PPP convergence is small for the horizontal component as well as on the first 10 min of the vertical component. The effect of the vertical component is significant in 15 to 40 min. When the elevation mask is 25° and 30°, it will significantly affect the multi-GNSS PPP convergence time for both the horizontal and vertical components.

When the elevation masks is 10°, within the confidence interval of 68.3%, the positioning accuracy of multi-GNSS PPP can reach decimeter levels of the horizontal and vertical components within five minutes. After 20 min of convergence, the positioning accuracy of the horizontal and vertical components can be superior to 10 cm, while be superior to 5 cm after 30 min. Within the confidence interval of 95%, the positioning accuracy of multi-GNSS PPP can be superior to 50 cm for the horizontal component and 60 cm for the vertical component. After 20 min convergence, the positioning accuracy can be superior to 20 cm for the horizontal and vertical components while be superior to 10 cm after 60 min. When the elevation masks is 30°, in the confidence interval of 68.3%, the positioning accuracy of multi-GNSS PPP can reach 40 cm for the horizontal and vertical components in five minutes. After 20 min of convergence, the positioning

Table 2 The maximum RMS and the RMS in the confidence interval of 95% and 99%

Elevation Masks	Confidence interval (95%)		Confidence interval (99%)		Maximum Value	
	H[cm]	U[cm]	H[cm]	U[cm]	H[cm]	U[cm]
10°	2.4	5.6	2.9	6.6	4.1	8.3
15 °	2.4	6.0	3.0	6.9	4.4	8.8
20 °	2.5	6.5	3.0	7.7	4.5	9.1
25 °	2.7	7.5	3.2	9.0	4.9	9.8
30 °	3.1	9.2	5.3	11.5	6.0	28.3

accuracy of the horizontal and vertical components can be superior to 15 cm, while be superior to 10 cm after 40 min. Within the confidence interval of 95%, the positioning accuracy of multi-GNSS PPP can be superior to 70 cm for the horizontal component and 80 cm for the vertical component within five minutes. After 30 min of convergence, the positioning accuracy can be superior to 20 cm for the horizontal and vertical components, while be superior to 10 cm for the horizontal component and 15 cm for the vertical component after 60 min.

The performance of the multi-GNSS kinematic PPP AR

The data of section 4.1 was used to analyze the performance of the multi-GNSS kinematic PPP AR. Firstly, the elevation masks was set to 10° for the PPP float solution to obtain the float ambiguities. Then different ambiguity subnets were selected to fix the ambiguities by setting the elevation masks of 10°, 15°, 20°, 25° and 30° respectively. The TTFF and the ambiguity fixing percentage were analyzed.

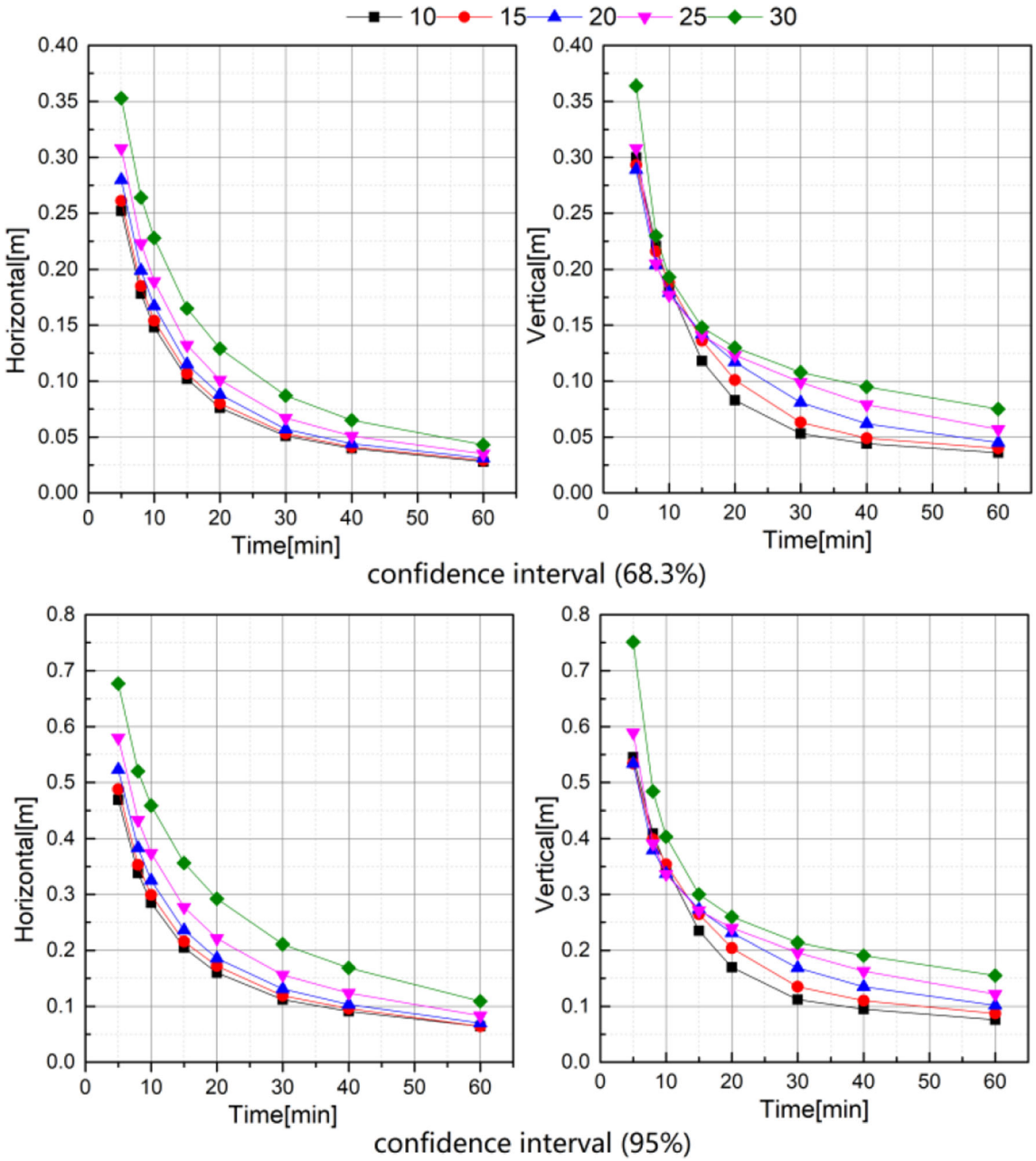

Fig. 4 The positioning accuracy of multi-GNSS PPP in the confidence interval of 68.3% and 95% after 5, 8, 10, 15, 20, 30, 40 and 60 min convergence with elevation masks of 10°, 15°, 20°, 25° and 30°

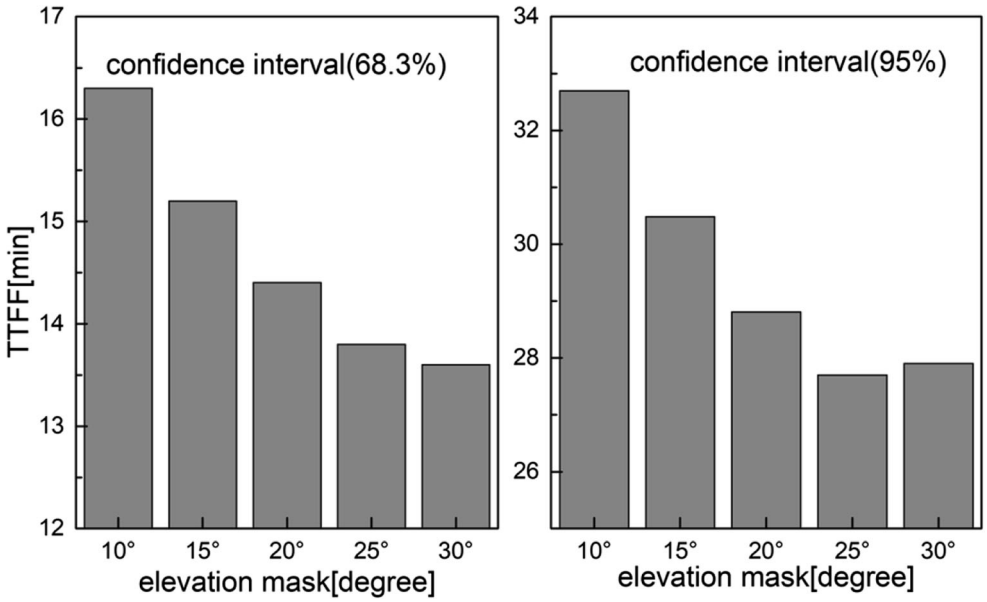

Fig. 5 The TTFF of multi-GNSS PPP AR of different elevation mask within the interval confidence of 68.3% and 95%

In this paper, the TTFF is defined as the time taken for the ambiguity to be firstly successfully fixed. Figure 5 shows the TTFF of the 90 individual stations in the confidence interval of 68.3% and 95%. As shown in Fig. 5, within the confidence interval of 68.3%, the TTFF decrease from 16.3 min to 13.6 min as the increase of elevation mask from 10° to 30° and the TTFF decrease obviously when the elevation mask below to 20°. However, within the confidence interval of 95%, when the elevation mask is 30°, the TTFF is large than that of the elevation is 25°.This is because the observations of the satellites with elevation mask below 20° have large noise and multi-path effect which decrease the accuracy of the float ambiguities. As the average PDOP is still 0.64 when the elevation mask reach to 20°. Therefore, if delete the satellites which the elevation mask is below to 20°, it will do helpful to the ambiguity fixing. But when the elevation mask is 30°, the PDOP can reach 2.3 for some stations, maybe the geometry is not very good and the ambiguities between different satellites have high correlation which is not good for ambiguity fixing.

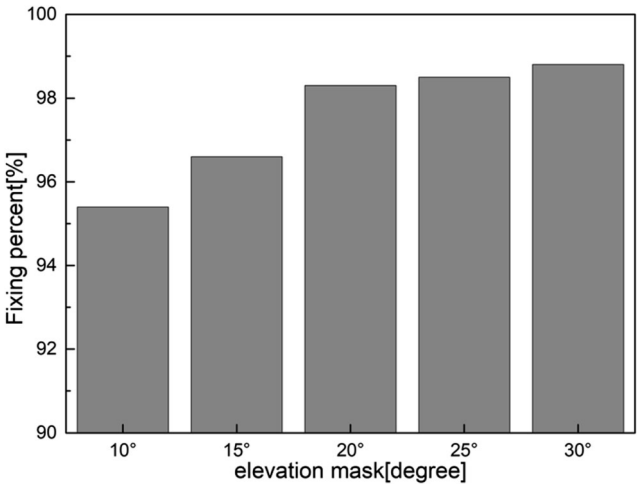

Fig. 6 The ambiguity fixing percentage of multi-GNSS PPP AR of different elevation mask

The ambiguity fixing percentage is an important indicator to assess the performance of PPP AR. The fixing percentage is defined as the percentage of fixed sessions over the total number of sessions. Figure 6 shows the average fixing percentage of different elevation mask. As shows in Fig. 6, the fixing percentage improves with the increasing of the elevation mask and when the elevation mask is below to 20°, the fixing percentage improves more obviously, from 95.4% to 98.3%. While when the elevation mask is large than 20°, the fixing percentage improvement is much smaller, only from 98.3% to 98.8%. This maybe because the environment for IGS track station is very good. The observation noise and multi-path effect is smaller when the elevation mask is large than 20° which will have less effect on ambiguity fixing.

Conclusions

This paper evaluated the impact of elevation mask on the performance of GPS + GLONASS+Galileo+BDS-2 + BDS-3 multi-GNSS kinematic PPP. Firstly, the PDOP characteristic of multi-GNSS and single-constellation with elevation masks of 10°, 15°, 20°, 25° and 30° were analyzed. Then, based on the data of 90 tracking stations of MGEX, the performance of multi-GNSS PPP with different elevation masks were analyzed. There were some preliminary results in our research. Firstly, the multi-GNSS PDOP varies little in different regions when the elevation mask is 5°. The PODP increases as the elevation mask increases. Fortunately, even

if the elevation mask is 30°, the PDOP of multi-GNSS is still about 95% less than 1.2, and the average PDOP is 0.82. Secondly, it will reduce the positioning accuracy and the convergence speed generally. However, when the elevation mask is below 25°, increasing the elevation mask has little effect on the position accuracy of the horizontal and vertical components in the first 10 min. But after 15 min, the effect on the vertical component became apparently. And after convergence, the RMS of multi-GNSS PPP can reach 5 cm and 10 cm for the horizontal and vertical components when the elevation mask is below 25°. When the elevation mask is 30°, the RMS is still less than 6 cm for the horizontal component, while about 99% of the RMS is less than 11.5 cm for the vertical component. Thirdly, for multi-GNSS PPP AR, it can improve the TTFF and the fixing percentage by fixing the ambiguity subnet with higher elevation mask firstly. Moreover, when the elevation mask is below to 20°, the improvement is more obvious and when the elevation mask is larger than 25°, the TTFF may become longer in some cases. Therefore, we suggest it is best to set the elevation mask to 20° for the multi-GNSS PPP AR.

Acknowledgments The IGS is acknowledged for providing high-quality precise orbit and clock corrections as well as tracking data. The Xiamen Xiang'an airport investment and Construction Co., Ltd. is acknowledged for providing tracking data.The Xiamen Key Laboratory of transportation infrastructure health and safety is acknowledged for providing project equipments.This work was partially supported by the National Natural Science Foundation of China (Grant No.41704033, Grant No.41704026), the Xiamen science and technology Program (Grant No.3502Z20193062) and the Natural Science Foundation of Jiangsu Province (Grant No.BK20191180).

References

An X, Meng X, Jiang W (2020) Multi-constellation GNSS precise point positioning with multi-frequency raw observations and dual-frequency observations of ionospheric-free linear combination[J]. Satellite Navigation. https://doi.org/10.1186/s43020-020-0009-x

Bisnath S, Gao Y (2008) Current State of Precise Point Positioning and Future Prospects and Limitations. In: Sideris MG (ed) Observing Our Changing Earth. Springer-Verlag, New York, pp 615–623

Böhm J, Niell A, Tregoning P, Schuh H(2006) Global mapping function (GMF): A new empirical mapping function based on numerical weather model data[J]. Geophys Res Lett 33(7). https://doi.org/10.1029/2005GL025546

Brack A, Günther C (2014) Generalized integer aperture estimation for partial GNSS ambiguity fixing[J]. J Geod 88(5):479–490

Cai C, Gao Y, Pan L, Zhu J (2015) Precise point positioning with quad-constellations: GPS, BeiDou, GLONASS and Galileo. Adv Space Res 56(1):133–143

Collins P, Lahaye F, Herous P, Bisnath S (2008) Precise point positioning with AR using the decoupled clock model. In: proceedings of the ION GNSS 2008, Savannah, 16–19 Sept, pp 1315–1322

Ge M, Gendt G, Rothacher M, Shi C, Liu J (2008) Resolution of GPS carrier phase ambiguities in precise point positioning (PPP) with daily observations. J Geod 82(7):389–399

Geng J, Shi C, Ge M, Dodson AH, Lou Y, Zhao Q, Liu J (2012) Improving the estimation of fractional-cycle biases for ambiguity resolution in precise point positioning. J Geod 86(8):579–589

Guo J, Li X, Li Z, Hu L, Yang G, Zhao C, Fairbairn D, Watson D, Ge M (2018) Multi-GNSS precise point positioning for precision agriculture. Precis Agric 19(5):895–911

Henkel P, Günther C (2012) Reliable integer ambiguity resolution: multi-frequency code carrier linear combinations and statistical a priori knowledge of attitude[J]. Navigation 59(1):61–75

Hu J, Zhang X, Li P, Ma F, Pan L (2020) Multi-GNSS fractional cycle bias products generation for GNSS ambiguity-fixed PPP at Wuhan University[J]. GPS Solutions 24:15. https://doi.org/10.1007/s10291-019-0929-9

Kouba J (2003) Measuring seismic waves induced by large earthquakes with GPS. Stud Geophys Geod 47(4):741–755

Laurichesse D, Mercier F, Berthias JP, Broca P, Cerri L (2009) Integer ambiguity resolution on undifferenced GPS phase measurements and its application to PPP and satellite precise orbit determination. Navigation 56(2):135–149

Leandro R, Santos M C, Langley R B (2006) UNB neutral atmosphere models: development and performance[C]//Proceedings of ION NTM. 52(1): 564–73

Li P, Zhang X (2014) Integrating GPS and GLONASS to accelerate convergence and initialization times of precise point positioning. GPS Solutions 18(3):461–471

Li X, Ge M, Zhang H, Wickert J (2013) A method for improving uncalibrated phase delay estimation and ambiguity-fixing in real-time precise point positioning. J Geod 87:405–416

Li X, Zhang X, Ren X, Fritsche M, Wickert J, Schuh H (2015) Precise positioning with current multi-constellation global navigation satellite systems: GPS, GLONASS, Galileo and BeiDou. Sci Rep 5:8328

Li X, Li X, Yuan Y, Zhang K, Zhang X, Wickert J (2018) Multi-GNSS phase delay estimation and PPP ambiguity resolution: GPS, BDS, GLONASS, Galileo. J Geod 92:579–608

Liu Y, Lou Y, Ye S, Zhang R, Song W, Zhang X, Li Q (2017) Assessment of PPP integer ambiguity resolution using GPS, GLONASS and BeiDou (IGSO,MEO) constellations. GPS Solutions 21(4):1647–1659

Lou Y, Zheng F, Gu S, Wang C, Guo H, Feng Y (2016) Multi-GNSS precise point positioning with raw single-frequency and dual-frequency measurement models. GPS Solutions 20(4):849–862

Montenbruck O, Steigenberger P, Prange L, Deng Z, Zhao Q, Perosanz F, Romero I, Noll C, Stürze A, Weber G, Schmid R, MacLeod K, Schaer S (2017) The multi-gnss experiment (mgex) of the international gnss service (igs)—achievements, prospects and challenges. Adv Space Res 59(7):1671–1697

Nadarajah N, Khodabandeh A, Wang KMC, Teunissen PJG (2018) Multi-GNSS PPP-RTK: from large- to small-scale networks. Sensors 18(4):1078

Parkins A (2011) Increasing GNSS RTK availability with a new single-epoch batch partial ambiguity resolution algorithm[J]. GPS Solutions 15(4):391–402

Rabbou MA, Elrabbany A (2017) Performance analysis of precise point positioning using multi-constellation GNSS: GPS, GLONASS, Galileo and BeiDou[J]. Surv Rev 49(352):39–50

Teunissen P (1995) The least-squares ambiguity decorrelation adjustment: a method for fast GPS integer ambiguity estimation. J Geod 70(1):65–82

Teunissen PJG (2007) Influence of ambiguity precision on the success rate of GNSS integer ambiguity bootstrapping[J]. J Geod 81(5):351–358

Teunissen P J G, Joosten P, Tiberius C C J M (1999) Geometry-free ambiguity success rates in case of partial fixing[J]. Proceedings of

the National Technical Meeting of the Institute of Navigation :201–207

Wang J, Feng Y (2013) Reliability of partial ambiguity fixing with multiple GNSS constellations[J]. J Geod 87(1):1–14

Wu JT, Wu SC, Hajj GA, Bertiger WI (1993) Effects of Antenna Orientation on GPS Carrier Phase[J]. Manuscripta Geodaetica 18: 91–98

Zumberge JF, Hefin MB, Jeferson DC, Watkins MM, Webb FH (1997) Precise point positioning for the efcient and robust analysis of GPS data from large networks. J Geophys Res Solid Earth 102(B3): 5005–5017

Publisher's note Springer Nature remains neutral with regard to jurisdictional claims in published maps and institutional affiliations.